The Linear-Phase Triangular Facet Approximation in Physical Optics Analysis of Reflector Antennas

W. A. Imbriale and R. E. Hodges
Jet Propulsion Laboratory
California Institute of Technology
4800 Oak Grove Drive
Pasadena, California 91109

Numerical analysis of reflector antennas uses a discrete approximation of the radiation integral. The calculation replaces the actual reflector surface with a triangular facet representation. The physical optics current is then approximated within each facet. This paper provides analytical details of the method based on the assumption of a constant magnitude and linear-phase approximation of the physical optics current. Example calculations are provided for parabolic, elliptical, and shaped subreflectors. The computed results are compared with calculations made using a constant-phase approximation. These results show that the linear-phase approximation is a significant improvement over the constant-phase approximation in that the solution converges over a larger angular region of space. This improvement can significantly reduce storage requirements and possibly execution speed.

I. Introduction

One of the simplest numerical techniques for electromagnetic scattering analysis is based on a discrete approximation of the physical optics (PO) radiation integral. The general modeling technique is similar to that employed by Rao et al. [1] for the moment method solution of electromagnetic scattering by surfaces of arbitrary shape. In this paper, we apply the methodology to the problem of shaped reflector antenna analysis. This calculation comprises two distinct approximations. First, the actual reflector surface is replaced by a triangular facet representation so that the reflector resembles a geodesic dome. One then makes an analytic approximation of the PO current within each of the facets. Upon evaluating the PO integral locally over each facet, the radiation integral reduces to a summation over the collection facets that represent the surface.

Several years ago, a computer program was developed at the Jet Propulsion Laboratory (JPL) utilizing the assumption of constant magnitude and phase of the PO current within each facet. This program has proven to be surprisingly robust and useful for the analysis of relatively small shaped reflectors, particularly when the near field is desired and surface derivatives are not known. It is natural to inquire whether a more sophisticated approximation of the PO surface current will yield more accurate results or permit the use of larger facets. In this paper, a linear-phase approximation of the surface currents is made. Within each triangular region, the resulting integral is written as the two-dimensional Fourier transform of the projected triangle. This triangular shape function can be integrated in closed form [2] and the complete PO integral is then a summation of these transforms. Significantly, other authors have developed more general techniques for performing the required integration [3,4,5], which could be very useful for future refinements.

In what follows, the explicit details of the analysis are provided along with example calculations of scattering from parabolic, elliptical, and shaped reflector surfaces. For a given size of triangular facet, two general trends emerge from the calculations. First, the linear-phase approximation takes about three times longer to compute a field point than does the constant-phase approximation. Second, there is an angular region of space over which the solution is valid, and this angular region is significantly larger with the linear-phase approximation than with the constant-phase approximation. Clearly, a trade-off situation exists here.

Since the surface geometry and PO currents must be stored in memory, the linear-phase approximation offers an advantage in terms of storage because fewer triangular facets are needed to reach convergence over a specified angular region. On the other hand, to claim a speed advantage, this method must reduce the required number of facets by at least one-third. This reduction will only be possible for reflectors in which relatively large regions can be adequately approximated by a uniformly illuminated planar surface. It has been found that this is the case for relatively large reflector antennas.

II. Analytical Details

The PO radiation integral over the reflector surface Σ can be expressed [6]

$$\mathbf{H}(\mathbf{r}) = -\frac{1}{4\pi}\int_{\Sigma}\left(jk+\frac{1}{R}\right)\hat{\mathbf{R}}\times\mathbf{J}_s(\mathbf{r}')\frac{e^{-jkR}}{R}ds' \tag{1}$$

in which $\mathbf{r}$ designates the field point, $\mathbf{r}'$ the source point, $R=|\mathbf{r}-\mathbf{r}'|$ is the distance between them, and $\hat{\mathbf{R}}=(\mathbf{r}-\mathbf{r}')/R$ is a unit vector. The PO surface current on the subreflector surface $\mathbf{J}_s$ is expressed

$$\mathbf{J}_s(\mathbf{r}') = 2\hat{\mathbf{n}}\times\mathbf{H}_s(\mathbf{r}') \tag{2}$$

For the purpose of analysis, the true surface Σ is replaced by a contiguous set of N-plane triangular facets. These facets, denoted Δ_i, are chosen to be roughly equal in size with their vertices on the surface Σ. Figure 1 shows a typical facet and its projection onto the x-y plane. Let (x_i, y_i, z_i) represent the *centroid* of each triangle where the subscript $i=1,\cdots,N$ is associated with a triangle. Then, the field obtained by replacing the true surface Σ by the triangular facet approximation is

$$\mathbf{H}(\mathbf{r}) = -\frac{1}{4\pi}\sum_{i=1}^{N}\int_{\Delta_i}\left(jk+\frac{1}{R}\right)\hat{\mathbf{R}}\times\mathbf{J}(\mathbf{r}')\frac{e^{-jkR}}{R}ds' \tag{3}$$

In Eq. (3), $\mathbf{J}$ is now the equivalent surface current evaluated on the triangular facets. Since the triangles are small, it is expected that $\hat{\mathbf{R}}$ and R do not vary appreciably over the area of a given facet. Thus, let $\hat{\mathbf{R}}_i$ and R_i be the value obtained at the centroid (x_i, y_i, z_i) of each facet and approximate Eq. (3) by

$$\mathbf{H}(\mathbf{r}) = -\frac{1}{4\pi}\sum_{i=1}^{N}\left(jk+\frac{1}{R_i}\right)\hat{\mathbf{R}}_i\times\mathbf{T}_i(\mathbf{r}) \tag{4}$$

$$\mathbf{T}_i(\mathbf{r}) = \int_{\Delta_i}\mathbf{J}_i(\mathbf{r}')\frac{e^{-jkR}}{R_i}ds' \tag{5}$$

Assume that the necessary transformations have been performed so that the incident field $\mathbf{H}_s$ is given in terms of the reflector coordinate system. Then

$$\mathbf{J}_i(\mathbf{r}') = 2\hat{\mathbf{n}}_i\times\mathbf{H}_s(\mathbf{r}') \tag{6}$$

Next, assume that the incident field can be represented by a function of the form

$$\mathbf{H}_s = \mathbf{h}_s(\mathbf{r}'_i)\frac{e^{-jkr_s}}{4\pi r_{si}} \tag{7}$$

where r_s is the distance to the source point. Also, $\mathbf{r}_i$ and $\mathbf{r}_{si}$ denote the vectors $\mathbf{r}'$ and $\mathbf{r}_s$ evaluated at the centroid of the ith triangular facet and are regarded as constants. Then, Eq. (5) can be written

$$\mathbf{T}_i(\mathbf{r}) = \frac{\hat{\mathbf{n}}_i \times \mathbf{h}_s(\mathbf{r}'_i)}{2\pi R_i r_{si}} \int_{\Delta_i} e^{-jk(R+r_s)} ds' \tag{8}$$

To simplify the form of the integration, the surface Jacobian is introduced within each triangular facet Δ_i. For a planar surface $z_i = f_i(x, y)$, a normal is given by

$$\mathbf{N}_i = -\hat{\mathbf{x}} f_{xi} - \hat{\mathbf{y}} f_{yi} + \hat{\mathbf{z}} \tag{9}$$

where

$$f_{xi} \equiv \frac{\partial f_i}{\partial x} \qquad f_{yi} \equiv \frac{\partial f_i}{\partial y}$$

and a unit normal is given by

$$\hat{\mathbf{n}}_i = \frac{\mathbf{N}_i}{|\,\mathbf{N}_i\,|} \tag{10}$$

This permits the explicit evaluation of the Jacobian as

$$J_{\Delta_i} = |\,\mathbf{N}_i\,| = \left[f_{xi}^2 + f_{yi}^2 + 1\right]^{1/2} \tag{11}$$

Making use of the Jacobian then allows Eq. (8) to be rewritten as

$$\mathbf{T}_i(\mathbf{r}) = \frac{\hat{\mathbf{n}}_i \times \mathbf{h}_s(\mathbf{r}'_i)}{2\pi R_i r_{si}} J_{\Delta_i} \int_{\Delta'_i} e^{-jk(R+r_s)} dx' dy' \tag{12}$$

in which Δ'_i represents the area of the ith triangular facet projected onto the $z = 0$ plane. Now, make a Taylor-series expansion of the exponent in Eq. (12). Retaining only the first-order terms, one can formally write

$$R(x, y) + r_s(x, y) = \frac{1}{k}(a_i - u_i x - v_i y) \tag{13}$$

in which a_i, u_i, and v_i are constants. This approximation corresponds to a far-field approximation on the ith triangle. With this approximation, Eq. (12) reduces to

$$\mathbf{T}_i(\mathbf{r}) = \frac{\hat{\mathbf{n}}_i \times \mathbf{h}_s(\mathbf{r}'_i)}{2\pi R_i r_{si}} J_{\Delta_i} e^{-ja_i} \int_{\Delta'_i} e^{j(u_i x' + v_i y')} dx' dy' \tag{14}$$

It may now be observed that this integral is the two-dimensional Fourier transform of the ith projected triangle Δ_i', expressed as

$$S(u,v) = \int_{\Delta_i'} e^{j(ux+vy)} dxdy \tag{15}$$

In order to explicitly evaluate the constants in Eq. (13), note that the equation of a plane can be expressed as

$$z = (x - x_i)f_{xi} + (y - y_i)f_{yi} + z_i$$

This can be used to obtain

$$a_i = kR(x_i, y_i) + kr_s(x_i, y_i) + u_i x_i + v_i y_i \tag{16}$$

$$\frac{u_i}{k} = \frac{(x_p - x_i) + (z_p - z_i)f_{xi}}{R(x_i, y_i)} + \frac{(x_s - x_i) + (z_s - z_i)f_{xi}}{r_s(x_i, y_i)} \tag{17}$$

$$\frac{v_i}{k} = \frac{(y_p - y_i) + (z_p - z_i)f_{yi}}{R(x_i, y_i)} + \frac{(y_s - y_i) + (z_s - z_i)f_{yi}}{r_s(x_i, y_i)} \tag{18}$$

Placing the result of Eq. (16) into Eq. (14), and recalling Eqs. (6) and (7), yields

$$\mathbf{T}_i(\mathbf{r}) = \mathbf{J}_i(r_i) J_{\Delta_i} e^{-j(u_i x_i + v_i y_i)} S(u_i, v_i) \frac{e^{-jkR_i}}{R_i} \tag{19}$$

This is the final form of the linear-phase approximation over each triangular facet. This expression can be used in Eq. (4) to compute the radiation integral once the Fourier transform of a triangular shape function $S(u,v)$ is known. Fortunately, this transform can be computed in closed form [2] from the expression

$$S(u,v) = \sum_{n=1}^{3} e^{j(ux_n + vy_n)} \frac{p_{n-1} - p_n}{(u + p_{n-1}v)(u + p_n v)} \tag{20}$$

in which (x_n, y_n) are the coordinates of the triangle vertices numbered in a clockwise direction. The slope of the nth side (between corners n and $n+1$) is given by

$$p_n = \frac{y_{n+1} - y_n}{x_{n+1} - x_n} \tag{21}$$

Some attention must be given to the following special cases. First, if $u = v = 0$, the transform reduces to the formula for the area of a triangle

$$S(0,0) = -\frac{1}{2}\Big[x_1(y_2 - y_3) + x_2(y_3 - y_1) + x_3(y_1 - y_2)\Big] \tag{22}$$

Next, if $u/v \rightarrow -p_n$, then

$$\lim_{u/v \rightarrow -p_n} S(u,v) = \frac{p_{n+1} - p_{n-1}}{v^2(p_{n+1} - p_n)(p_{n-1} - p_n)} \times \left[e^{j(ux_{n-1} + vy_{n-1})} - e^{j(ux_n + vy_n)} \right] + \frac{(x_{n+1} - x_n)}{jv} e^{j(ux_n + vy_n)} \tag{23}$$

III. Numerical Results

A FORTRAN subroutine was written to perform the linear-phase calculations indicated above. Test cases were run for parabolas, ellipses, and shaped subreflectors, and the results were compared with calculations that use a constant magnitude and phase approximation on the triangular facets. A focused parabola is neither an interesting nor a challenging case for the algorithm, since the phase variation over the facet is small. As a simple test case, the far-field pattern and gain of a $1,000\lambda$-diameter parabolic reflector with a focal length of $F = 400\lambda$ was calculated. The reflector is illuminated by a linearly polarized horn with a $\cos\theta$ pattern function. Figure 2 compares the linear- and constant-phase approximation for a roughly equally spaced 80-by-80 rectangular grid of points divided into triangles over the reflector surface (approximately 10,000 triangles). The running time on a Cray X-MP/18 was less than one minute. Convergence was checked by increasing the number of triangles until the computed solution did not change appreciably over the angular region of interest. It has been previously demonstrated [7,8,9] that, once sufficient triangles to converge the solution have been utilized, the results of the constant-phase algorithm are valid, so only comparisons of the two techniques are presented.

A more interesting example is the ellipse shown in Fig. 3. The projected aperture of the ellipse is about 3 m, illumination function is a $\cos^{42}\theta$ pattern function (22.3-dB gain), and the frequency is 31.4 GHz. The ellipse is about 350λ along the major axis. Figure 4 compares the constant-phase approximation for different grid densities of approximately 4,000, 10,000, and 23,000 triangles, and illustrates a general trend of the method, i.e., depending on the size of the triangles, there is an angular limit over which the solution is valid. Figure 5 compares the linear-phase approximation with the constant-phase approximation for the 4,000-triangle case and demonstrates that the angular range is larger with the linear-phase approximation.

A third example is the shaped subreflector shown in Fig. 6. The diameter is 3.42 m (135 in.), and it is fed with a $\cos^{233}\theta$ pattern function (29.7-dB gain). Figure 7 compares the results of a 4,000- and 10,000-triangle grid constant-phase approximation with a 4,000-triangle linear-phase approximation. The frequency of operation is 2.3 GHz, hence, the subreflector is about 26λ in diameter. The 10,000-triangle constant phase is the converged result and the 4,000-triangle linear case gives the same result. A very good approximation is also obtained with a 1,400-triangle grid for the linear case, but no meaningful results are obtained with the constant-phase case. Figure 8 gives the linear-phase result for 31.4 GHz (360λ subreflector) using 23,000 triangles. No meaningful result is obtained for the equivalent constant-phase case.

One final example is given by a beam-waveguide system that has recently been built at JPL. The measurement setup consists of a 22-dB-gain feedhorn that is used to illuminate a beam-waveguide system consisting of a pair of parabolic reflectors. The mirrors are arranged to replicate the input feed pattern at the focal point of the second dish. Details of the geometry are given elsewhere [10]. A calculation of this system was made using the triangular facet PO technique by first computing the near-field scattering from the first reflector and using these values to compute the PO current on the second reflector. Subsequently, the triangular facet program is used a second time to compute the field radiated by the second parabolic reflector. In Fig. 9, the results of this calculation are compared with experimental measured data taken at X-band. As can be seen, the computed results compare favorably with the measured data.

Most of the examples given are for large reflectors to illustrate the robust character of the technique. For smaller reflectors ($< 100\lambda$), meaningful results can be obtained on a typical desktop computer in a reasonable time.

IV. Conclusions

The triangular facet approximation technique provides a simple and flexible method of analysis for reflector antennas. We have found that the linear-phase approximation is valid over a larger angular region than is the constant-phase approximation. In applying this method to fairly large (100 to 1000λ) reflectors, the linear-phase approximation provides a significant reduction in the computer storage requirements and can reduce computation time in some cases.

Acknowledgment

The research described in this paper was carried out by the Jet Propulsion Laboratory, California Institute of Technology, under a contract with the National Aeronautics and Space Administration. Reference herein to any specific commercial product, process, or service by trade name, trademark, manufacturer, or otherwise, does not constitute or imply its endorsement by the United States Government or the Jet Propulsion Laboratory, California Institute of Technology.

References

[1] S. M. Rao, D. R. Wilton, and A. W. Glisson, "Electromagnetic Scattering by Surfaces of Arbitrary Shape," *IEEE Trans. Antennas and Propagation*, vol. AP-30, no. 3, pp. 409–418, May 1982.

[2] S. W. Lee and R. Mittra, "Fourier Transform of a Polygonal Shape Function and Its Application in Electromagnetics," *IEEE Trans. Antennas and Propagation*, vol. 31, no. 1, pp. 99–103, January 1983.

[3] W. B. Gordon, "Far-Field Approximations to the Kirchoff-Helmholtz Representation of Scattered Fields," *IEEE Trans. Antennas and Propagation*, vol. 23, no. 4, pp. 590–592, July 1975.

[4] J. S. Asvestas, "Line Integral and Physical Optics, Part I: The Transformation of the Solid-Angle Surface Integral to a Line Integral," *J. Opt. Soc. A.*, vol. 2, no. 6, pp. 891–895, June 1985.

[5] J. S. Asvestas, "Line Integral and Physical Optics, Part II: The Conversion of the Kirchoff Surface Integral to a Line Integral," *J. Opt. Soc. A.*, vol. 2, no. 6, pp. 896–902, June 1985.

[6] A. W. Rudge, K. Milne, A. D. Olver, and P. Knight, *The Handbook of Antenna Design, Vol. I*, London: Peter Peregrinus, 1982.

[7] V. Galindo-Israel, T. Veruttipong, and W. Imbriale, "GTD, Physical Optics and Jacobi-Bessel Diffraction Analysis of Beamwaveguide Ellipsoids," *AP-S International Symposium*, Philadelphia, Pennsylvania, pp. 643–646, 1986.

[8] T. Veruttipong, J. R. Withington, V. Galindo-Israel, W. A. Imbriale, and D. A. Bathker, "Design Considerations for Beamwaveguide in the NASA Deep Space Network," *IEEE Trans. Antennas and Propagation*, vol. AP-36, no. 12, pp. 1779–1787, December 1988.

[9] A. G. Cha and W. A. Imbriale, "New Analysis of Beamwaveguide Antennas Considering the Presence of the Metallic Tube and Its Experimental Verification," *AP-S International Symposium*, Dallas, Texas, pp. 1506–1509, 1990.

[10] J. R. Withington, W. A. Imbriale, and P. Withington, *JPL Beam Waveguide Test Facility*, to be presented at the 1991 International IEEE Antennas and Propagation Society Symposium, June 24, 1991.

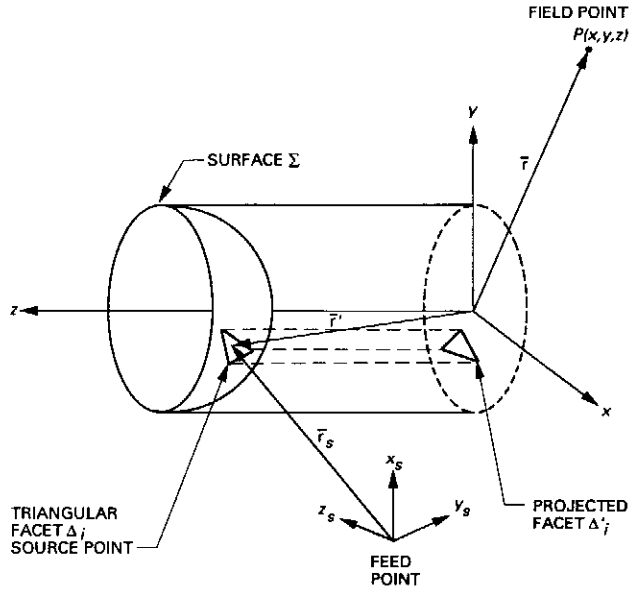

Fig. 1. Reflector analysis coordinate systems and a typical triangular facet.

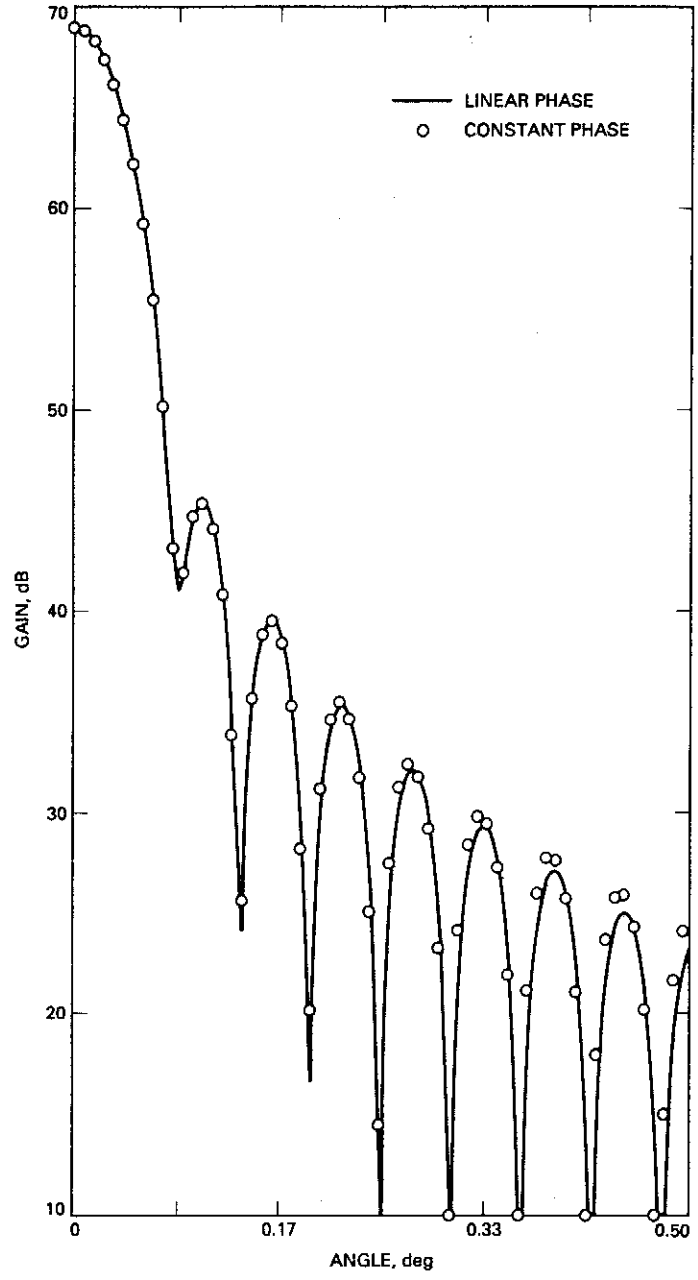

Fig. 2. Parabolic example.

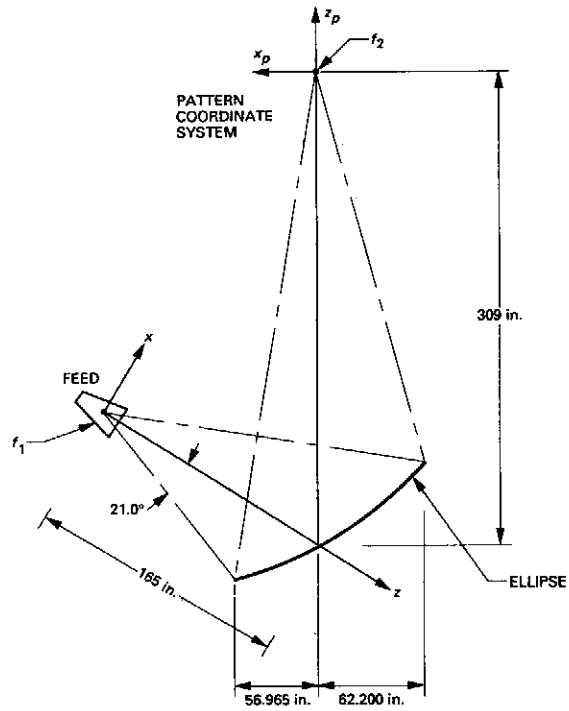

Fig. 3. Ellipse geometry.

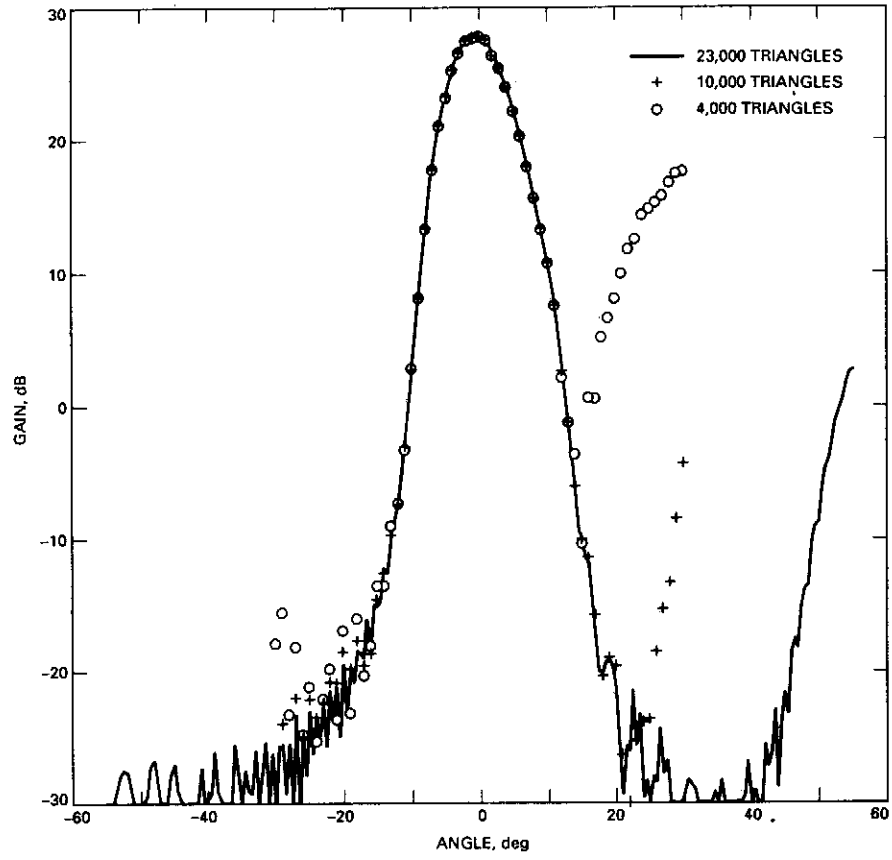

Fig. 4. Ellipse example: constant-phase approximation for offset plane.

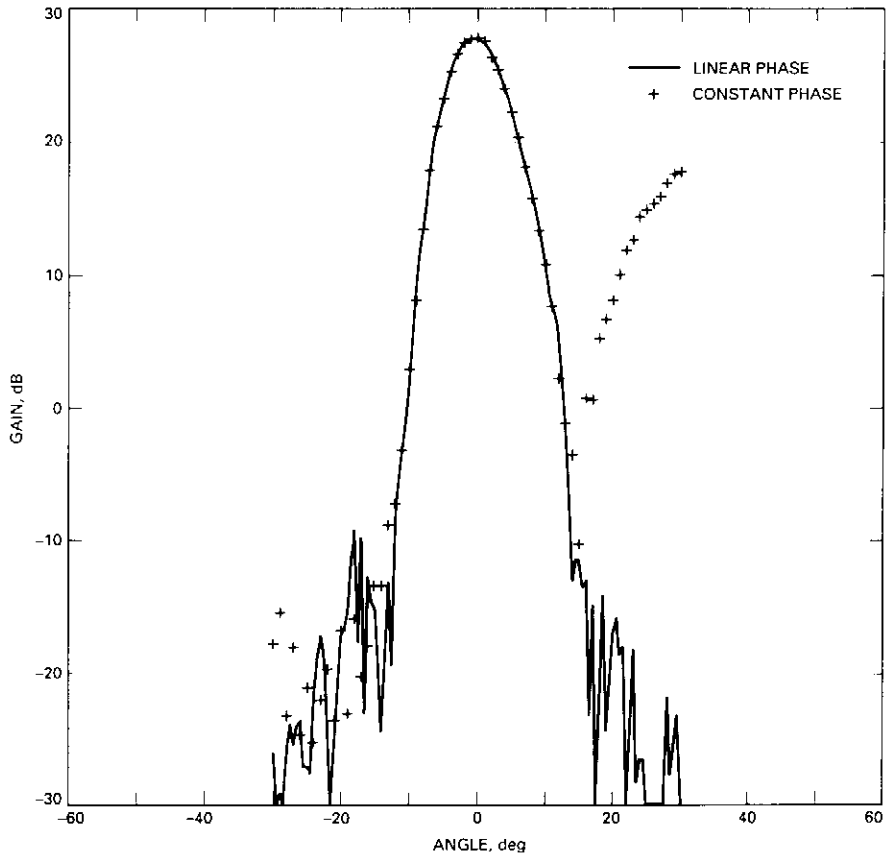

Fig. 5. Ellipse example: constant versus linear phase for offset plane.

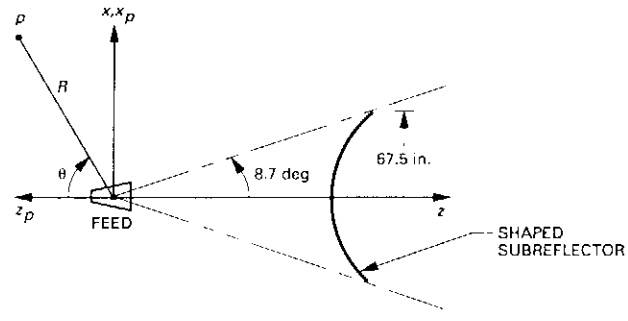

Fig. 6. Shaped subreflector geometry.

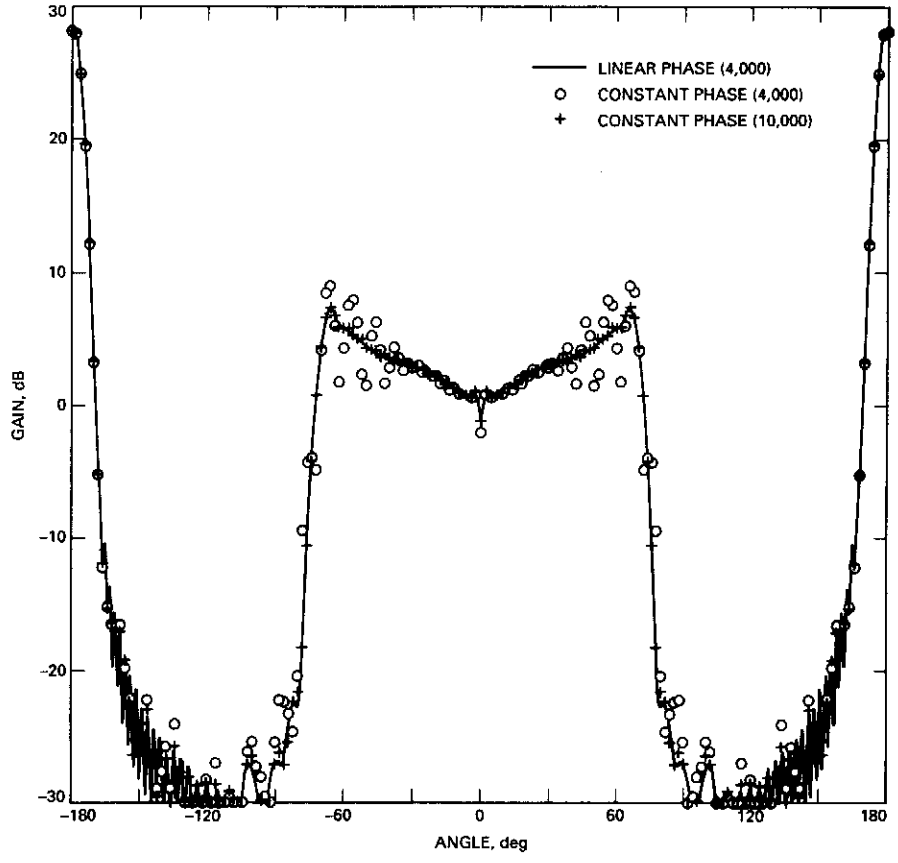

Fig. 7. Shaped subreflector example for H-plane at 2.3 GHz.

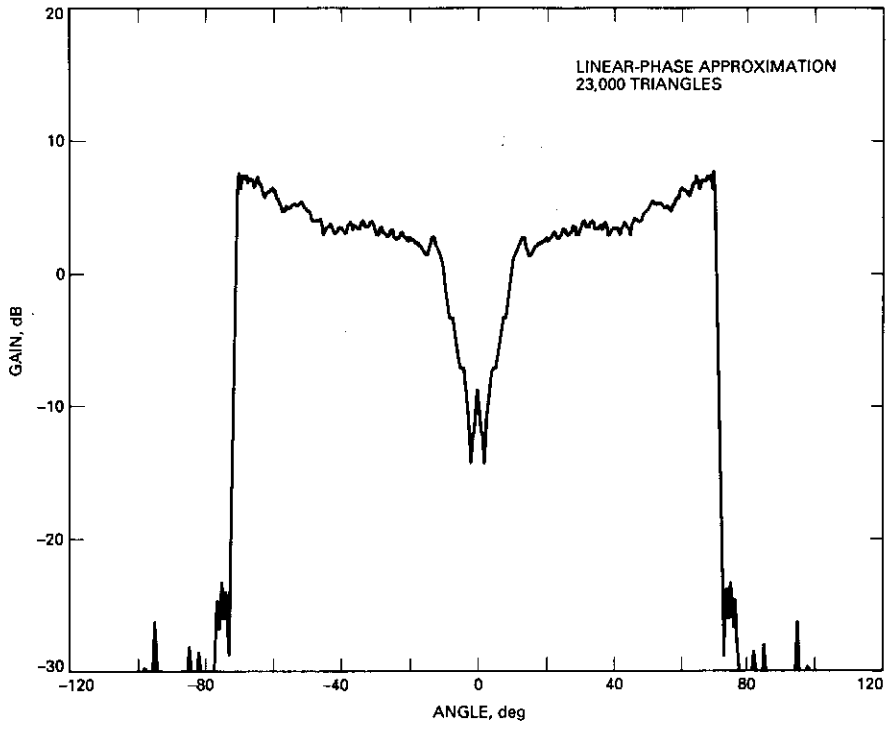

Fig. 8. Shaped subreflector, 31.4 GHz.

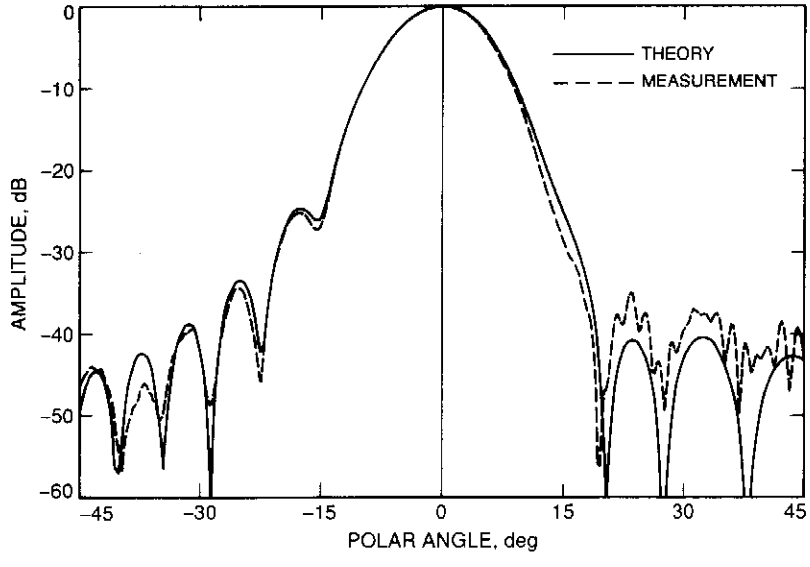

Fig. 9. Two-mirror X-band beam waveguide.